Reconciling Space Object Observed and Solar Pressure Albedo-Areas Via Astrometric and Photometric Data Fusion

Moriba K. Jah, Ph.D.[1]
The University of Texas at Austin
Vishnuu Mallik[2]
The University of Texas at Austin

ABSTRACT

There are many Resident Space Objects (RSOs) in the Geostationary Earth Orbit (GEO) regime, both operational and debris. The primary non-gravitational force acting on these RSOs is Solar Radiation Pressure (SRP), which is sensitive to the RSO's area-to-mass ratio. Sparse observation data and mismodelling of non-gravitational forces has constrained the state of practice in tracking and characterizing RSOs. Accurate identification, characterization, tracking, and motion prediction of RSOs is a high priority research issue as it shall aid in assessing collision probabilities in the GEO regime, and orbital safety writ large. Previous work in characterizing RSOs has taken a preliminary step in exploiting fused astrometric and photometric data to estimate the RSO mass, shape, attitude, and size. This works, in theory, since angles data are sensitive to SRP albedo-area-to-mass ratio, and photometric data are sensitive to shape, attitude, and observed albedo-area. By fusing these two data types, mass and albedo-area both become observable parameters and can be estimated as independent quantities. However, previous work in mass and albedo-area estimation has not quantified and assessed the fundamental physical link between SRP albedo-area and observed albedo-area. The observed albedo-area is always a function of the SRP albedo-area along the line of sight of the observer. This is the physical relationship that this current research exploits.

1. BACKGROUND AND MOTIVATION

Advances in space technology, coupled with an increased dependence on space-based assets for both military and commercial purposes has led to a dramatic increase in the space object (SO) population since the first man-made object, Sputnik, was launched. A majority of these space objects consist of inactive satellites and debris that have been created due to collisions, explosions, and components breaking off over time due to space object aging (RSO gerontology). The Space Surveillance Network currently maintains a catalog of over 23,000 objects that are larger than 10 cm in diameter all the way up to the International Space Station. Only about 1500 of these objects are active space assets. Due to the need for meeting safety requirements for manned spaceflight, the debris population in low Earth orbit (LEO) has gained much of the research focus thus far. This, along with the fact that the LEO debris population can be studied from both radar and optical observations, has allowed researchers to achieve some meaningful understanding of the space environment and force models that govern the behavior of LEO space debris [1]. However, there is still work to be done for characterizing the debris population and environment in higher Earth orbits. Due to the larger search space, limited observations, and limitations in sensor technology, it is a non-trivial task to detect, track, and characterize debris in higher Earth orbits, let alone, be able to accurately predict their long-term orbital motion and behavior. Fig. 1 shows data obtained from the Defense Advanced Research Projects Agency's (DARPA) Space Surveillance Telescope. The data demonstrates that although a large number of objects have been detected in high Earth orbits, there remains a significant population of objects that have not been correlated to known objects, hence demonstrating that there are gaps in the current body of knowledge and the techniques used to study space objects, that need to be filled. In other words, detecting an object and tracking an object are not equivalent. Tracking an object requires that the object be (a) detected and (b) uniquely identified, making tracking at best as difficult as detection and at worse much more challenging.

In order to know something, one must measure it, and in order to understand it, one must predict it. To that end, one

[1] Associate Professor, Aerospace Engineering and Engineering Mechanics Department, Cockrell School of Engineering, The University of Texas at Austin, Austin, TX 78712

[2] Graduate Student, Aerospace Engineering and Engineering Mechanics Department, Cockrell School of Engineering, The University of Texas at Austin, Austin, TX 78712

of the major capabilities that needs to be filled is the accurate modelling of non-gravitational forces acting on objects in the near-Geostationary Earth Orbit (GEO). Such non-gravitational forces include Solar Radiation Pressure (SRP), Thermal Emissions, Outgassing, and Electromagnetic interactions. SRP is the primary non-gravitational force acting on objects in GEO, and improved modelling of SRP shall enhance the ability to predict the behavior and the spatio-temporal evolution of RSOs in the near-GEO regime. Improved characterization of RSOs entails acquiring improved estimates of an RSO's physical features, such as mass, area, shape and size. Previous work [2] in this area has shown that under idealized assumptions it is possible to infer an object's mass and albedo-area through the mutual information content obtained by fusing astrometric and photometric data. The research results provided here builds upon work done by [2], extending it to using physically consistent BRDF models for both the acceleration due to SRP formulation and the light curve formulation. The need for this was recognized in Ref. 5. The current research also exploits the physical link between the albedo area estimated through the dynamic mismodelling of SRP and the observed albedo area obtained directly via the measured light curve data.

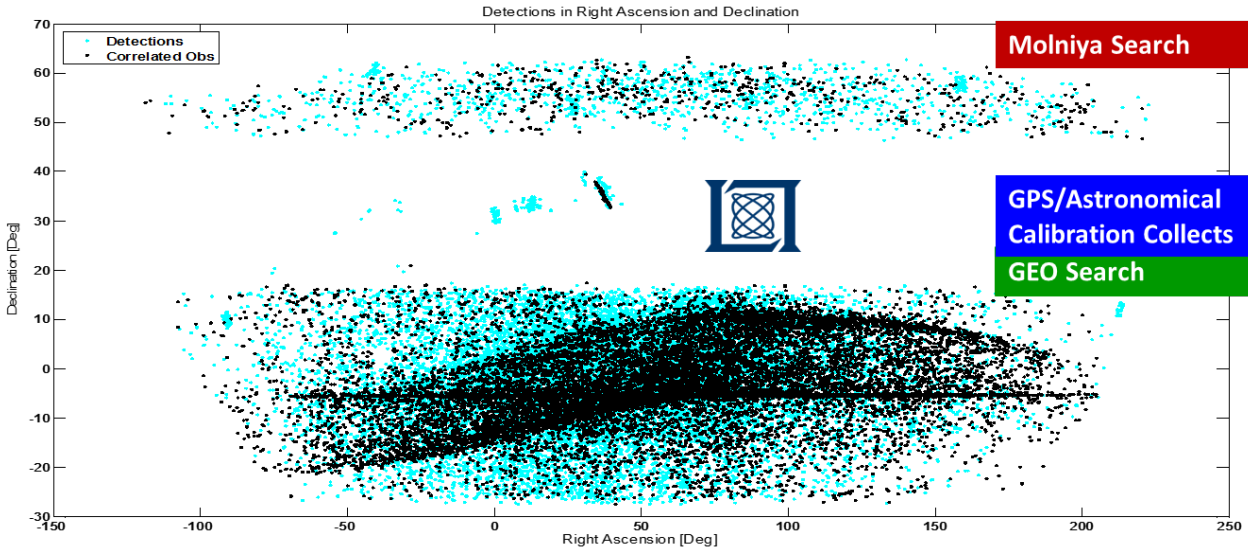

Fig. 1. Space Surveillance Telescope Synoptic Search Data. Tracked objects are shown in black, and detected objects (i.e. objects of unknown identity) are shown in Cyan. Image courtesy of MIT Lincoln Laboratory.

2. DATA FUSION

Space Situational Awareness (SSA) involves the acquisition of information regarding the space environment, particularly man-made space objects, and the ability to understand and predict their behavior in order to ensure safety and security of active space assets [3]. Data fusion is a methodology that enables SSA, as it extracts knowledge gained from the mutual information of multiple sources to achieve refined estimates of position and identity of a space object [4]. For the characterization and feature estimation problem, it is only through the fusion of astrometric and photometric data that one can estimate features such as mass, as has been shown by [2]. This is due to the underlying physics behind these two data types: Astrometric or angles data are sensitive to SRP albedo-area-to-mass ratio, and hence this quantity is observable from this data type. Photometric or light curve data are sensitive to the object's shape, attitude, and observed albedo-area properties. Using only a single one of these data types in the estimation process does not make mass an observable quantity, since otherwise mass cannot be separated from the albedo-area. However, by fusing the two data types, mass can be estimated separately because the observed albedo-area is always a function of the SRP albedo-area onto the observer's line of sight vector to the SO [2] as shall be subsequently derived and shown.

3. ALBEDO-AREA FROM SRP AND LIGHT CURVES: THE PHYSICAL CONNECTION

In general, the SRP is the main perturbing non-gravitational force experienced by objects at an altitude over 1000 km. The force due to SRP has a complex formulation that depends on the attitude of the space object and its distance from the sun, as well as the geometry and optical properties of each surface of the object. It is caused by the net effect of absorption, reflection, and transmission of photons striking and leaving the space object. Fig. 2 depicts the geometry

of reflection from a single facet [5], where $\hat{N}$ is the normal unit vector to the surface of the facet, $\hat{I}$ is the unit vector from the center of the facet to the illumination source (oriented at angle θ_i from $\hat{N}$), $\hat{O}$ is the unit vector from the center of the facet to the observer (oriented at angle θ_r from $\hat{N}$), $\hat{H}$ is the half angle (bisector) vector between the illumination source and observer unit vectors. $\hat{X}$ and $\hat{Y}$ are unit vectors that describe the attitude of the surface in the body frame of the SO. The angle between the illumination source, the object, and the observer is termed as the phase angle, δ.

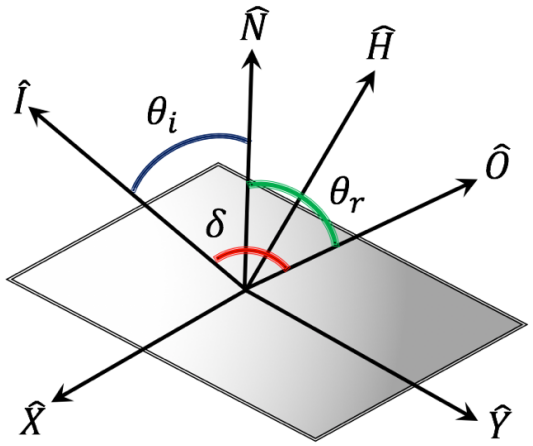

Fig. 2. Geometry of reflection from a single facet.

Fig. 3. depicts the reflection geometry from a surface of a single facet due to incoming radiation. This particular representation is for the case of Lambertian diffuse and near-specular reflection. Here, $\hat{R}$ is the direction of perfect "mirror-like" specular reflection, and the conical lobe around it depicts the lobe of near-perfect specular reflection due to material properties and irregularities. Part of the radiation that is incident on the surface is directly absorbed by the surface, and the momentum imparted by the photons that are absorbed into the surface causes a force in the direction of incident radiation. The incident radiation that is not absorbed by the surface is reflected, partly in a specular manner, and partly in a diffuse manner. The intensity and geometry of the specular and diffuse reflection depend on the material and surface properties of the reflecting surface, and the momentum exchanged caused due to photons reflected specularly and diffusely cause a net diffuse and specular force on the surface, the direction of which depends on the geometry of reflection and ratios of specular to diffuse reflectivities. For the case shown in Fig. 3., the near-perfect specular reflection causes a net force in the direction opposite to the surface normal, and the Lambertian diffuse reflection causes a force that is partly in the direction of incident radiation and partly in the direction opposite to the surface normal. The total force on a surface due to incoming radiation is hence the net force from the absorbed, specular, and diffuse reflection, which causes a net acceleration. In the development of SRP acceleration used for the research presented here, a similar approach as Ref. [6] is followed, where transmissivity is assumed to be zero[3], and the coefficient of absorptivity, specular reflectivity, and diffuse reflectivity are related by the following constraint:

$$\alpha + \rho + \delta = 1 \tag{1}$$

where α is the coefficient of absorption, ρ is the coefficient of specular reflection, and δ is the coefficient of diffuse reflection.

[3] i.e. in future work to be handled via the modeling of a Bidirectional Transmission Distribution Function [BTDF]

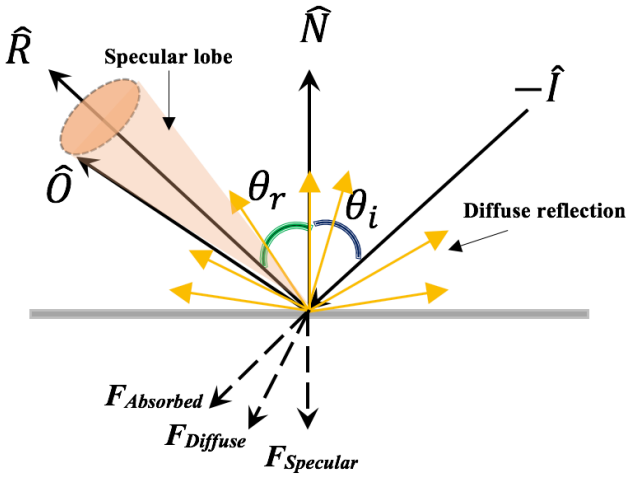

Fig. 3. Reflection geometry and forces due to incident radiation off a single facet.

In its most general form, the acceleration due to SRP can be written as cf. [5]

$$a_{SRP} = -\sum_{i=1}^{N_{facets}} \int_0^{\infty} \frac{F_k(\lambda) A_i f_i (\hat{I}.\hat{N}_i)_+}{mc} \left(\hat{I} + \left(\int_0^{2\pi} \int_0^{\pi/2} f_r \cos\theta_r \hat{O} d\theta_r d\phi_r \right)_i \right) d\lambda . \tag{2}$$

This formulation models the surface of the SO as a combination of N number of facets, and hence the total acceleration due to SRP is expressed as a sum of the acceleration over all the facets. In the above expression, f_r is the Bidirectional Reflectance Distribution Function (BRDF), where

$$f_r = \left(dR_d + sR_s \right). \tag{3}$$

In Eq. (3), dR_d is the diffuse bidirectional reflectance distribution, and sR_s is the specular bidirectional reflectance distribution. The total BRDF is calculated as the sum of these two quantities, which are both dependent on the illumination source and direction, the observer direction, and the surface properties of the object. The BRDF defines how incoming photons interact with and reflect from any given surface of an object, and is an integral term of the SRP formulation. The dependence on the SOs attitude is indirectly incorporated into the BRDF formulation through the illumination and observer direction.

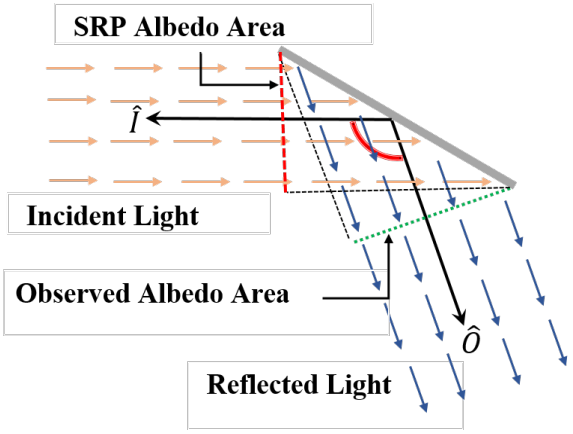

Fig. 4. Reflection from a single facet, showing SRP albedo area and observed albedo area (right).

The BRDF is also essential in modelling photometric data, or light curves. A light curve can be described as the temporal history of an object's wavelength-dependent observed brightness, or apparent magnitude [7]. The observed brightness of an object is a function of the number and direction of the photons that are reflected off the surface, which itself is a function of the illumination source, the number and direction of the incoming photons, and the wavelength(s) being measured by the sensor used to observe it. Light curves can be used to model the observed brightness of an object given the object's shape, size, and attitude, by representing the physics that determines the object's reflectance properties, i.e. a BRDF. Essentially, a light curve model uses a BRDF and information about the object's features to determine the number of photons that are reflected in the direction of the observer. This in combination with atmospheric extinction, for example, will determine the notional quantities of photons that can be measured. Using a similar formulation as Ref [7], a general analytical light curve model is given by

$$m_{object} = m_{sun} - 2.5\log_{10}\left(\sum_{i=1}^{N_{facets}} \frac{f_r A_i \left(\hat{N}_i \cdot \hat{I}\right)\left(\hat{N}_i \cdot \hat{O}\right)}{r^2}\right) \tag{4}$$

where m_{sun} is the apparent magnitude of the sun for a given band pass (which in the case of visible light is -26.7), and r is the distance between the RSO and the observer. It is important to note that to accurately model both the acceleration due to SRP, and light curves for an object, the same BRDF must be used in both formulations because how a surface scatters energy is independent of a passive observer. Examining the formulations shown in Eq. (2) and Eq. (4) along with Fig. 4, it is intuitive that the SRP albedo-area to mass ratio, which is observable through astrometric data, is a function of the SOs albedo-area projected along the direction of the Sun, while the albedo-area observed through the light curve data is a function of the SRP albedo-area along the line of sight of the observer. This relationship is the main physical relationship that this work exploits, and is shown in Fig. 4 to provide more clear insight.

As shown in Fig. 4, the phase angle is the angle between the unit vector from the SO along the line of sight of the observer and the unit vector from the SO in the direction of the Sun. The albedo-areas estimated through the fusion of these two data types should have better agreement at lower phase angles. In terms of albedo-area, this physical relationship (in theory) can be written as

$$K_{SRP} = C_R A_i \cos\theta_i \tag{5}$$

and

$$K_{OBS} = C_R A_i \cos\theta_i \cos\theta_r \tag{6}$$

where C_R is the total albedo of the surface of an RSO, and K_{SRP} and K_{OBS} are the SRP albedo-area and observed albedo-area, respectively. Eq. (5) can hence be written as a function of the Observed albedo-area, Eq. (6), through

$$\frac{K_{OBS}}{\cos\theta_r} = K_{SRP} \tag{7}$$

At lower phase angles, the SRP albedo-area and observed albedo area should have better agreement, and in theory, at 0 degree phase angle, the two are exactly the same. In other words, at very low phase angles, the light curve data provide a direct measurement of the SRP albedo-area.

4. METHODOLOGY

4.1 SRP FORMULAITON

The RSO used in this study is modelled as an object whose surface reflectance properties can be represented using a BRDF that has a Lambertian diffuse component and a perfeclty specular or 'mirror-like' component. Such a BRDF is given by [5]

$$f_r = d\left(\frac{\rho}{\pi}\right) + s\left(\frac{F_0 \delta\left(\hat{O} - \hat{R}\right)}{\cos\theta_i}\right) \tag{8}$$

The general SRP formualtion shown in Eq. (2) can be analytically solved for this BRDF, and results in the acceleration due to SRP having the form [5]

$$a_{SRP} = -\sum_{i=1}^{N_{facets}} \frac{F_{sun} A_i (\hat{I}.\hat{N}_i)_+}{mc}\left((1 - s_i F_0)\hat{I} + \left(\frac{2}{3}d\rho + 2 s_i F_0 \left(\hat{I}\cdot\hat{N}_i\right)\right)\hat{N}_i\right) \tag{9}$$

which is the acceleration due to SRP model used for facet-based modelling of spacecraft [8]. This formulation is based on the acceleration due to the differential force from the incident radiation, specular reflection, and diffuse reflection.

4.2 ANALYTICAL LIGHT CURVE FORMULATION

Light cuves were generated in the visible-light bandpass by computing the apparent brightness magntiude of the object in the direction of the obsever through Eq. (4). The BRDF in Eq. (8) is used as the BRDF for this light curve modelling in the estimation filter to ensure physcial consistency between the acceleration due to SRP formulation and the light curve formulation. However, the BRDF in Eq. (8) is slightly modified for our purpose, since in its orginial form, the specular component only cotnributes when the phase angle is 0 degrees, or when the normal and bisector vectors are aligned, which results in glints. From a practical standpoint, the specular component contributes to the total BRDF when the $\hat{O}$ and $\hat{R}$ direction are less than or equal to about 10 degrees. Hence, in its modifed form, the BRDF we use for light curve modelling in the filter for this work is given by

$$f_r = d\left(\frac{\rho}{\pi}\right) + s\left(\frac{F_0 H\left(\hat{O}, \hat{R}\right)}{\cos\theta_i}\right) \tag{10}$$

where

$$H\left(\hat{O}, \hat{R}\right) = \begin{cases} 1 & a\cos\left(\hat{O}\cdot\hat{R}\right) \le 10^\circ \\ 0 & a\cos\left(\hat{O}\cdot\hat{R}\right) > 10^\circ \end{cases}. \tag{11}$$

This modification essentially creates a specular lobe when the angle between the direction of the observer and the direction of mirror like reflection is less than 10 degrees, which given the subject matter expertise of others in the community, is not unreasonable.

4.3 FILTERING TECHNIQUE

An unscaled Unscented Kalman Filter (UKF) was used in the estimation process. The algorithm was developed following a similar approach as taken by Ref. [9] in the deveopment of the Unscented Schmidt-Kalman Filter algorithm. The unscaled version of the UKF only differs from the scaled or more common version of the UKF by the fact that the mean value of the estimated parameters is eliminated from the sigma points, which in turn eliminates the tuning parameters. The lack of tuning parameters eliminates the complexity of correclty tuning the regular scaled UKF, and has shown better performance in processing real data [9].

The estimated state paramaters are

$$\hat{X} = \begin{bmatrix} R & V & b_{Kdiff} & m & \vdots & b_{Kspec} \end{bmatrix} \tag{12}$$

Where R and V are the position and velocity states of the RSO, b_{Kdiff} and b_{Kspec} are proxy values for diffuse and specular albedo-area of the RSO, and m is the mass of the SO. Proxy values are chosen following a similar procuedure as described by [10] to constrain the sigma points of K_{diff} and K_{spec} to be positive. The albedo-area's can be broken down and written in terms of the diffuse and specular reflectivity terms as

$$K_{diff} = d\rho A_i \tag{13}$$

$$K_{spec} = sF_0 A_i . \tag{14}$$

For this work, the specular contribution to the albedo-area is only being estimated when the condition stated in Eq. (11) is met and is otherwise treated as a "consider" term, since the specular term only contributes to the apparent magnitude when the condition for a glint is met or the phase angle is less than 10 degrees. By treating K_{spec} as a "consider" parameter for the times when there is no specular contribution to albedo-area, we are able to analyze how including this parameter's uncertainty may affect the results of the estimation process, but not actually allow estimates of the parameter itself to affect our results since the value for this parameter is not updated in the corrective step of the filtering process.

Using this notation in Eq. (4) and Eq. (8), the model used to estimate light curve data in the filter can be written in the form

$$m_{object} = m_{sun} - 2.5\log_{10}\left(\sum_{i=1}^{N_{facets}} \frac{F_{rA_i}\left(\hat{N}_i \cdot \hat{I}\right)\left(\hat{N}_i \cdot \hat{O}\right)}{r^2} \right) \tag{15}$$

where

$$F_{rA_i} = \frac{K_{diff}}{\pi} + \frac{K_{spec}}{\cos\theta_i} \tag{16}$$

is the combination of the BRDF (f_r) and facet Area (A_i) terms. Similarly, the model used to estimate the acceleration due to SRP in the filter, which is given by Eq. (9), can be written as

$$a_{SRP} = -\sum_{i=1}^{N_{facets}} \frac{F_{sun}(\hat{I}.\hat{N}_i)_+}{mc} \left(\left(A_i - K_{spec}\right)\hat{I} + \left(\frac{2}{3}K_{diff} + 2K_{spec}\left(\hat{I} \cdot \hat{N}_i\right) \right)\hat{N}_i \right) \tag{17}$$

This formulation allows the albedo-areas estimated through the acceleration due to SRP by the filter to be fed in as an input into the estimated light curve measurement model, thereby ensuring consistency in albedo-areas. However, as can be seen in Eq. (17), it is not possible to separate the acceleration due to the $A_i\hat{I}$ term and write it as a function of specular and diffuse reflectance's. It is in the scope of future work to investigate this and derive a solution, but for this work, the true area of each facet is used for the A_i term, since this parameter shows poor observability when estimating albedo-area as well [2].

Along with light curve data, angles data in the form of azimuth (az) and elevation (el) are also used, and hence the measurement vector for the filter is given by

$$\hat{y} = \begin{bmatrix} m_{object} & az & el \end{bmatrix} \tag{18}$$

5. SIMULATIONS AND RESULTS

The RSO used for this work was modeled as 3-axis stabilized rectangular cuboid with its $\hat{Y}$ axis pointed towards the Sun direction vector and $\hat{X}$ axis in the plane of the orbit, and the $\hat{Z}$ axis completing a dextral reference frame. The physical properties of the RSO are provided in Table 1.

Table 1. RSO physical and surface reflectance parameters

Parameter	Value
Mass	1000 kg
[height, length, width]	[8m, 8m, 8m]
d	0.8
s	0.2
ρ	0.6
F_o	0.6
K_{diff}	30.72 m^2
K_{spec}	7.68 m^2

Reference data were generated every 60 seconds for a total of 15 days starting Dec 21, 2010 at 05:00:00 UT from Maui, Hawaii. Data were only collected for a period of 12 hours a day. The initial conditions of the RSO under study are given by the Keplerian elements a = 42364.1932 km, e = 0.001, i = 2 degrees, M_0 = 0, ω = 0, Ω = 0. Table 2 provides details of the simulated reference measurements as well as the measurement model used in the filter, and Table 3 lists the initial errors for each estimated parameter in the filter.

Table 2. Reference data and filter measurement noise settings

Parameter	Reference data measurement noise	Filter measurement noise
m_{object}	0.1	0.2
az	1 arc second	2 arc seconds
el	1 arc second	2 arc seconds

Table 3. Initial errors in estimated parameters

Parameter	Initial Error
Position	100 km in X, Y, and Z
Velocity	0.1 km/s in X, Y, Z
Mass	800 kg
K_{diff}	13.81 m^2
K_{spec}	2.54 m^2

Fig. 5 through Fig. 12 show results for two different simulation cases: 1) In the first case, both angles and light curve data were used in the estimation process. 2) In the second case, only angles data were used and light curve data were neglected. The UKF works well for large yet realistic initial errors (100 km in position, 0.1 km/s in velocity). The results clearly show that mass and albedo-area estimation is only possible through the data fusion approach, and by neglecting light curve data, mass and albedo-area are not observable parameters. With the data fusion approach, the filter is able to recover mass from an initial error of 800 kg and estimate it to within 13 kg 3σ uncertainty and an RMS of 2.6 kg. K_{diff} is also precisley estimated with an RMS of 0.035 m^2 and 3 m^2 3σ uncertainty. K_{spec} is estimated with an RMS of 0.15 m^2 and 3.1 m^2 3σ uncertainty. Note that in all the plots, the RMS values indicated are calculated only after the filter has converged to steady state values, which in this case was 3000 samples of data or about 4 days from the simulation epoch.

Table 4. 3σ uncertainties for position and velocity estimates.

Error	X 3σ	Y 3σ	Z 3σ
Position	33 m	31 m	18 m
Velocity	1.8 mm/s	2.9 mm/s	1.3 mm/s

Table 5. 3σ uncertainties for mass and albedo-area estimates.

Error	3σ
Mass	13 kg
K_{Diff}	3 m^2
K_{Spec}	3.1 m^2

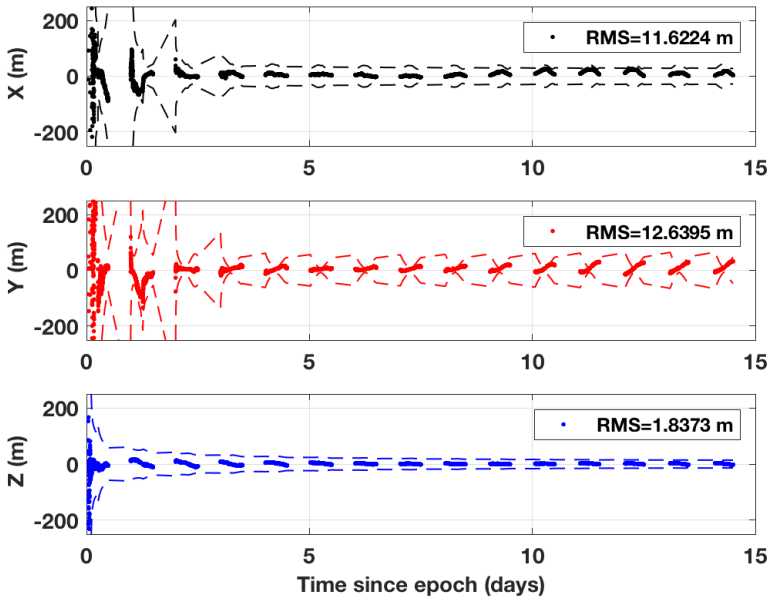

Fig. 5. Position errors with 3σ covariance envelopes.

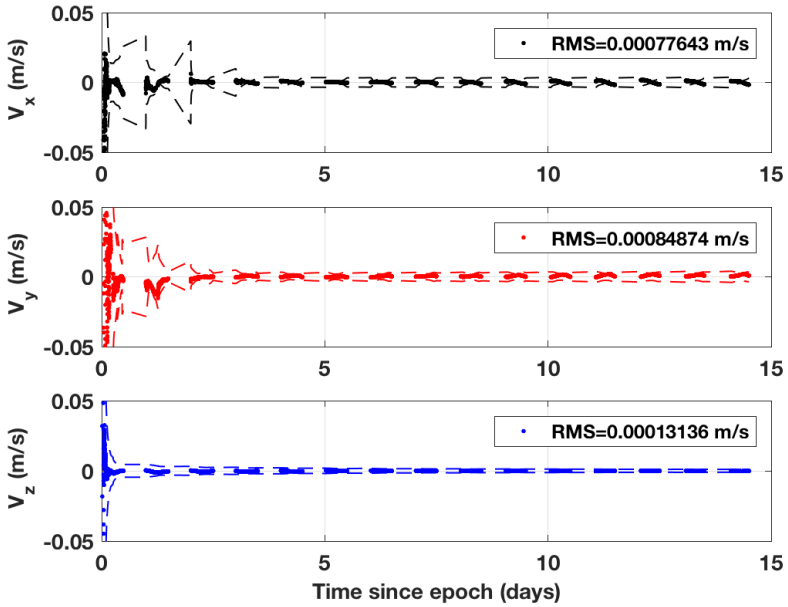

Fig. 6. Velocity errors with 3σ covariance envelopes.

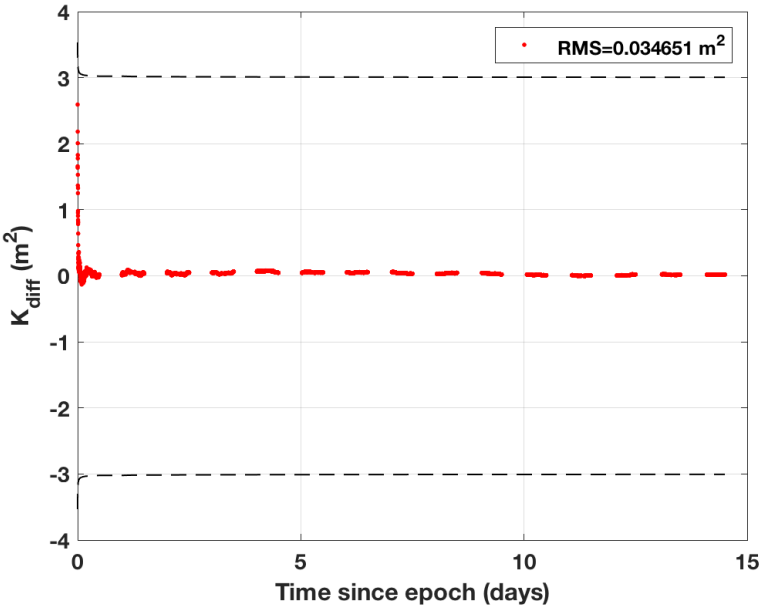

Fig. 7. Diffuse Albedo-Area estimate with data fusion.

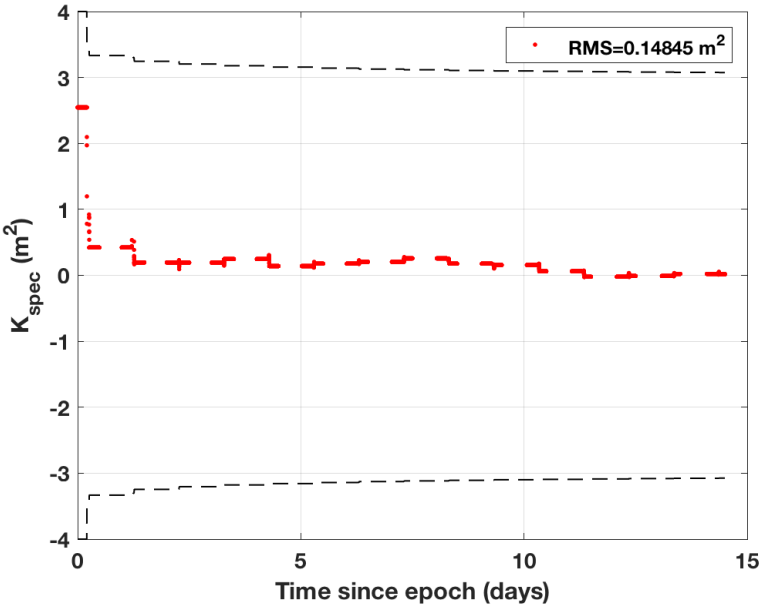

Fig. 8. Specular Albedo-Area estimate with data fusion.

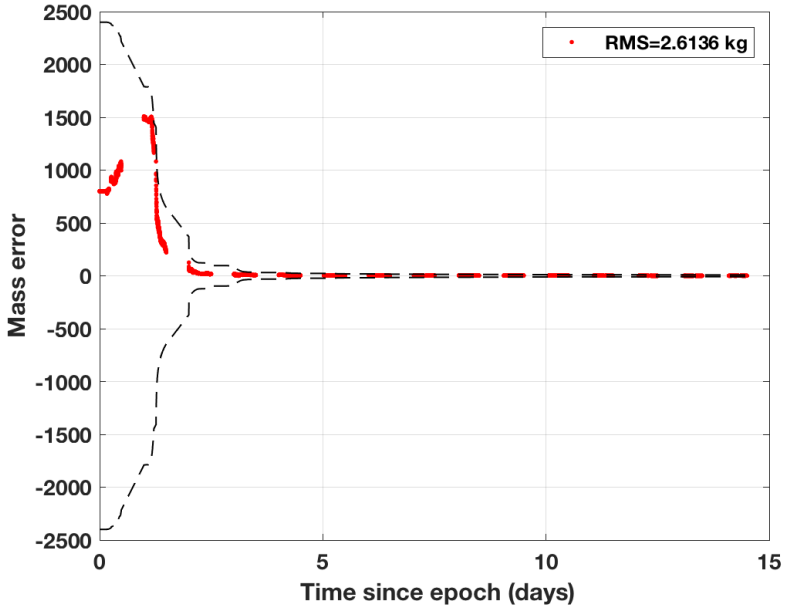

Fig. 9. Mass estimate with data fusion.

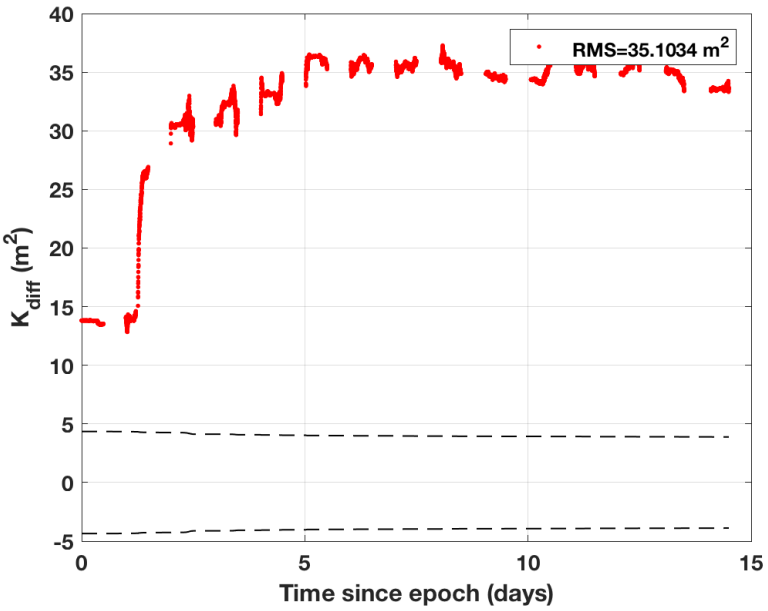

Fig. 10. Diffuse Albedo-Area estimate with astrometric data only.

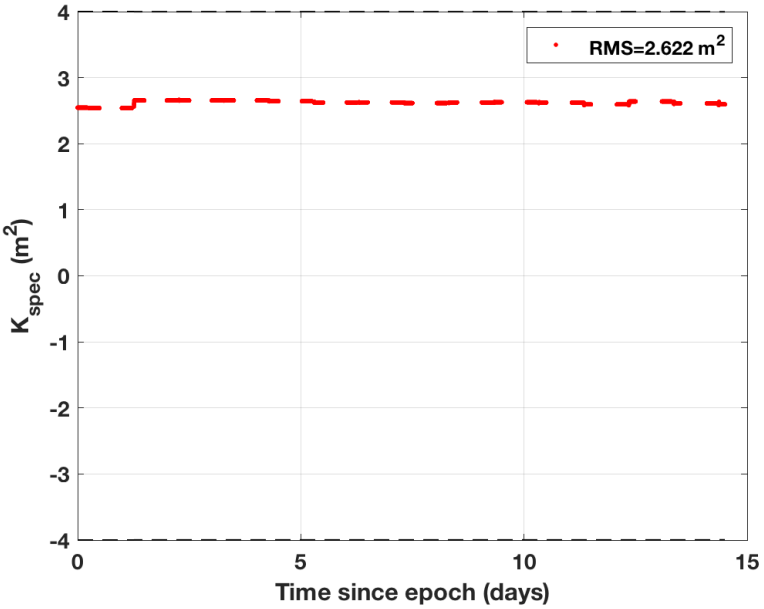

Fig. 11. Specular Albedo-Area estimate with astrometric data only.

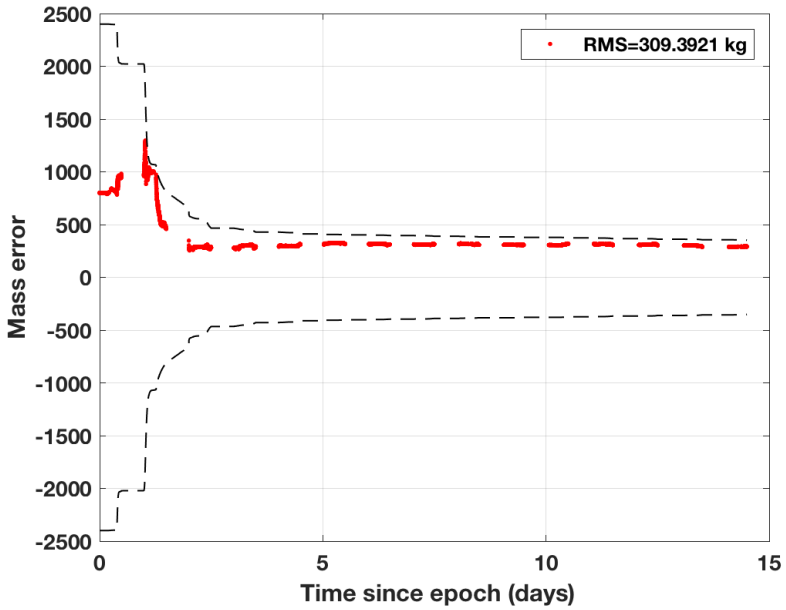

Fig. 12. Mass estimate with astrometric data only.

With reference to Fig. 12., it is worth mentioning that although the filter seems to estimate some of the SO mass, this should not be interpreted as such because mass is not observable as an independent quantity within the angles-only data. Thus, the mass estimated by the filter with angles-only data is really the average albedo-area-to-mass ratio of the SRP.

Fig. 13 shows the relative difference in the Fisher Information (FI) for K_{spec} and mass for the two simulation cases, with case 2 (angles data only simulation) treated as the reference in calculating relative difference. From these plots, we are able to quantify information content and reinforce the fact that the information content for mass and K_{spec} contained in both angles and light curve data is orders of magnitude more than the information content contained in just angles data, which supports why mass and albedo-area are not observable through angles data alone. From Fig.

13, we can also get some idea of the data sensitivity to phase angle. For specular albedo-area, we observe a rise in Fisher Information content at phase angles less than 10 degrees, which makes physical sense since the specular component of the BRDF only starts contributing to the total BRDF at lower phase angles. For mass, we notice that the information content is maximum at higher phase angles, but also shows a rise in values at lower phase angles, revealing that there is some information content that can be exploited and used to the advantage of getting more precise estimates of mass.

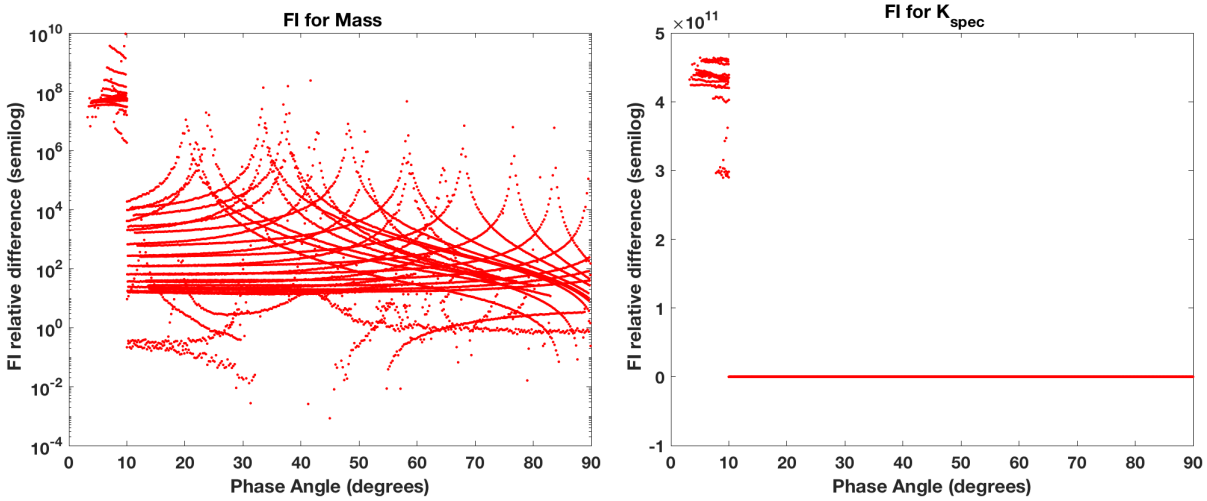

Fig.13. Relative difference in Fisher Information for K_{spec} (right) and mass (left) between Case 1 (Data fusion approach) and Case 2 (astrometric data only).

6. FUTURE WORK

The work presented here was performed as a proof of concept and the simulations were idealized in the sense that the attitude was assumed to be known and was not estimated, the RSO model considered was simple and had one of its sides pointed at the Sun at all times, and a simple BRDF formulation was used for deriving the synthetic light curves and acceleration due to SRP. Future work would entail the following steps to create high-fidelity results with a more realistic scenario:

1. Estimating the RSO's attitude for the case of a non 3-axis stabilized attitude profile.
2. Using a more sophisticated RSO model, such as a box wing with solar panels or other more representative RSO shape.
3. Using other BRDFs such as Maxwell-Beard and Cook-Torrance that may be more representative of common GEO RSO material and surface properties, and using the approach developed used by [5,11] to model solar radiation pressure for refined BRDF models.
4. Glint Analysis: Glints occur when the bisector vector and the normal are close to each other and/or at low phase angles. During glints, an object's brightness as viewed by the observer is dominated by its surface's specular reflectance properties, which causes sudden change in the apparent brightness of the object. Glints contain significantly higher information content about the objects surface and material properties, and this information content can be used in the estimation process to aid the RSO characterization effort.
5. Modelling the force caused due to the incident irradiance in the acceleration due to SRP formulation as a quantity that is dependent on other estimated parameters, hence allowing the single area term that cannot be written as a function of albedo to be estimated as well.

7. CONCLUSIONS

This work provides insight into the underlying physics that connects the albedo-area as seen by the observer to the SRP albedo-area. There is a physical connection between SRP albedo-area which drives SRP forces and torques experienced by a given space object, and its observed albedo-area. The net SRP force is caused due to absorption and reflection (diffuse and/or specular) of incident radiation from the surface of an object. If we ignore the contribution of transmissivity, the total energy exchanged due to absorption and reflection can be constrained to unity and this

constraint can be exploited. The physical connection between SRP and Observed albedo-area then allows us (in theory) to estimate the space object's mass, only observable by way of the mutual information contained in combined astrometric and photometric data. It is important that the SRP force model use the same BRDF as the observed albedo-area measurement formulation.

The results showed promising scope for future work, as precise estimates of both mass and albedo-area could be attained even under large uncertainties in the RSO's position, velocity, and mass.

8. ACKNOWLEDGEMENTS

The authors would like to thank Dr. Tamara Payne for useful discussions on some of the topics addressed in this work.

9. REFERENCES

[1] Schildknecht, T., Musci, R., Ploner, M., Beutler, G., Flury, W., Kuusela, J., de Leon Cruz, J., de Fatima Dominguez Palmero, L., "Optical observations of space debris in GEO and in highly-eccentric orbits." *Advances in Space Research*, vol. 34, no. 5, 2004, pp. 901–911.

[2] Linares, R., Jah, M., Crassidis, J., Leve, F., Kelecy, T., "Astrometric and Photometric Data Fusion for Inactive Space Object Feature Estimation". *Journal of the International Academy of Astronautics: Acta Astronautica*, vol. 99, pp. 1-15.

[3] Joint Chiefs of Staff. Space Operations. Joint Publication 3-14, May 2013.

[4] Jah, M. and Madler, R., "Satellite Characterization: Angles and Light Curve Data Fusion for Spacecraft Stat and Parameter Estimation," Proceedings of the Advanced Maui Optical and Space Surveillance Technologies Conference, Vol. 49, Wailea, Maui, HI, Sept. 2007.

[5] Wetterer, C., Linares, R., Crassidis, J., Kelecy, T., Ziebart, M., Jah, M., P. Cefola., "Refining Space Object Radiation Pressure Modeling with Bidirectional Reflectance Distribution Functions." *AIAA Journal of Guidance, Control, and Dynamics*, vol. 37, No. 1, 2013, pp. 185-196.

[6] Lyon, R. H., *Geosynchronous Orbit Determination Using Space Surveillance Network Observations and Improved Radiative Force Modeling*, Masters thesis, Massachusetts Institute of Technology, 2002.

[7] Wetterer, C. J. and Jah, M., "Attitude Estimation from Light Curves", *Journal of Guidance, Control and Dynamics*, vol. 32, No. 5, 2009, pp. 1648-1651.

[8] Ziebart, M., "Generalized Analytical Solar Radiation Pressure Modeling Algorithm for Spacecraft of Complex Shape". *Journal of Spacecraft and Rockets*. vol. 41, no. 5, 2004, pp. 840–848.

[9] Stauch, J. and Jah, M., "Unscented Schmidt-Kalman Filter Algorithm", *Journal of Guidance Control and Dynamics*, vol. 38, No.1, 2015, pp.117-123

[10] Wetterer, C. J., Crassidis, J. L., Linares, R., Chow, C. C., and Jah, M. K., "Simultaneous Position, Velocity, Attitude, Angular Rates, and Surface Parameter Estimation Using Astrometric and Photometric Observations," Proceedings of the FUSION Conference, Istanbul, Turkey, July 2013.

[11] Linares, R., Crassidis, J. L., Wetterer, C. J., Hill, K., and Jah, M. K., "Astrometric and Photometric Data Fusion for Mass and Surface Material Estimation using Refined Bidirectional Reflectance Distribution Functions-Solar Radiation Pressure Model," Advanced Maui Optical and Space Surveillance (AMOS) conference, Wailea, Maui, HI, September 2013.